Adsorbent screening for airborne BTEX analysis and removal

Irene Lara-Ibeas, Cristina Megias-Sayago, Alberto Rodríguez-Cuevas, Rubén Ocampo-Torres, Benoît Louis, Stéphane Colin, Stéphane Le Calvé

ADSORBENT SCREENING FOR AIRBORNE BTEX ANALYSIS AND REMOVAL

Irene Lara-Ibeas[1,2], Cristina Megías-Sayago[3], Alberto Rodriguez-Cuevas[4], Rubén Ocampo-Torres[1], Benoît Louis[3], Stéphane Colin[2], Stéphane Le Calvé[1,4,*]

[1] ICPEES – Institut de Chimie et Procédés pour l'Energie, l'Environnement et la Santé, Atmospheric Physical Chemistry Team, UMR 7515 CNRS – Université de Strasbourg – ECPM, 25 rue Becquerel F-67087 Strasbourg cedex 2, France

[2] Institut Clément Ader (ICA), Université de Toulouse/CNRS, INSA, ISAE-SUPAERO, Mines-Albi, UPS, 31400 Toulouse, France

[3] ICPEES – Institut de Chimie et Procédés pour l'Energie, l'Environnement et la Santé, Energy and Fuels for a Sustainable Environment Team, UMR 7515 CNRS – Université de Strasbourg – ECPM, 25 rue Becquerel F-67087 Strasbourg cedex 2, France

[4] In'Air Solutions, 25 rue Becquerel, 67087 Strasbourg, France

***** slecalve@unistra.fr; Tel.: +33-3-6885-0368

Abstract

Adsorption is a commonly used technique for removal and analysis of gaseous pollutants due to its cost efficiency at low concentrations. In this work, single and competitive BTEX adsorptions were studied on three non-porous, mesoporous and microporous commercial adsorbents, namely Carbopack® B, SBA-16 and HKUST-1, respectively. For all these materials, C_8 aromatics were preferentially adsorbed, preventing in some cases the adsorption of the most volatile species, i.e. benzene and toluene. This behavior indicates that the competition phenomenon is closely related to the strength of adsorbate-adsorbent interactions. Activation energies for the desorption process were determined to be 33.8 and 33.7 and 35.9 kJ/mol for Carbopack® B, SBA-16 and HKUST-1, respectively, demonstrating that

stronger interactions are present in microporous materials. Among the investigated adsorbents, SBA-16 seems to be the best candidate for air treatment and analysis since it exhibited high adsorption capacity, moderate hydrophobicity, minimal roll-up and low activation energy for the desorption. The experimental results obtained illustrate the complexity of multicomponent adsorption process on materials with different porosity and surface chemistry.

Keywords: Adsorption, BTEX, air pollution, desorption, air treatment

1. INTRODUCTION

Benzene, Toluene, Ethylbenzene and Xylenes isomers (BTEX) are a group of highly volatile gaseous pollutants frequently found in indoor [1]–[4] and outdoor air [5], [6]. It is known from the literature that these compounds have a negative impact on the environment since they contribute to the formation of ozone and other photochemical oxidants [7]. Moreover, BTEX are either known for being, or suspected to be, irritants, neurotoxins, allergens or carcinogens [8] and their exposure on a long term basis presents a serious threat to the human health [9], [10]. Therefore, implementing effective strategies for pollution control is of paramount importance to limit human exposure and prevent the environment degradation.

Nowadays, numerous techniques based on physicochemical or biological processes have been developed for gaseous pollutant's removal such as thermal, plasma, catalytic or photocatalytic oxidation, condensation, membrane separation, biological degradation, absorption and adsorption [11]–[13]. However, the pollutant concentration in indoor air or industrial environments is relatively low, ranging from sub ppb level to a hundred of ppm. It is worthy to mention that not all removal techniques can be effective at such low concentration ranges [14]. Furthermore, some of these methods are expensive or require regular maintenance limiting their use at domestic scale. Among them, adsorption has been demonstrated to be a technique that exhibits a good compromise between cost and efficiency for BTEX removal at low concentrations.

At the same time, analytical methods such as gas chromatography are required to monitor air quality and/or control the efficiency of the aforementioned depollution techniques. Since BTEX concentrations are usually very low, the integration of preconcentration devices is generally needed to increase the sensitivity of these methods. Thus, in the mentioned preconcentration unit, an adsorbent is used to trap pollutant molecules and concentrate the sample that will be, subsequently, analysed by conventional gas chromatography. The adsorbent requirements in pollutant removal as well as gas analysis include a minimal breakthrough, large adsorption capacity, thermal stability and selectivity to the targeted pollutants. Additionally, the desorption temperature should be moderate to enable an effective, inexpensive and rapid adsorbent regeneration.

In this regard, several materials differing in structure, porosity and surface chemistry have been lately investigated. Among these materials, carbon-based materials have been addressed as VOC/BTEX adsorbents including activated carbons [15], [16], ordered mesoporous carbons [17] or carbon nanotubes [18]. However, graphitised carbon blacks, typically employed for sampling [19] and gas analysis [20] applications, have been scarcely evaluated in terms of adsorption capacity. In contrast, BTEX adsorption capacity of a wide variety of silicas have been extensively studied as shown in Table 1. Multiple silica structures such as SBA-15, MCM-41, MCM-48, KIT-6 or SiO_2 exhibited significant adsorption abilities ranging from 15.78 to 415.39 mg/g towards benzene and toluene. Several MOF have been also employed for VOC adsorption studies [21]–[24]. More precisely, HKUST-1 have been widely investigated for the adsorption of various aromatic compounds such as benzene, toluene, p-xylene and o-xylene (see Table 2).

Despite the huge number of BTEX adsorption related studies to date, most of them have been conducted at very high concentrations (5300 – 800000 ppm) as recently reported by Szulejko *et al.* [25]. Nevertheless, there is a lack of studies employing more realistic BTEX concentrations, ranging from 0.5 to 99 ppm [26]–[28].

Table 1. Summary of former studies on benzene and toluene adsorption on various types of silicas

Silica type	S_{BET} (m^2/g)	V_{total} (mL/g)	V_{micro} (mL/g)	D_{meso} (Å)	Compound	Concentration (ppm)	Temperature (°C)	Adsorption Capacity (mg/g ads)	Reference
SBA-16	572	0.72	-	3.4 and 6.0	Toluene	100	23	24.88	This work
SBA-15	698	1.2	0.07	6.3	Benzene	1000	--	71.08	[29]
MCM-41	1088	0.92	-	2.9	Benzene	1000	--	79.67	[29]
MCM-48	1210	1.02	-	2.4	Benzene	1000	--	76.55	[29]
KIT-6	912	1.29	0.13	6.3	Benzene	1000	--	98.42	[29]
SBA-15-1	612	1.00	0.05	5.6	Toluene	71.65	30	147.39*	[28]
SBA-15-2	596	0.84	0.06	6.55	Toluene	71.65	30	190.74*	[28]
MCM-41	538	0.64	-	2.38	Toluene	71.65	30	130.05*	[28]
SiO_2	558	0.8	-	4.33	Toluene	71.65	30	86.70*	[28]
SBA-15	501	1.143	-	8.15	Benzene	1000	20	15.78	[30]
SBA-15 A	495	0.54	0.089	5.58	Toluene	n. a.	25	167.42	[31]
SBA-15 B	715	0.77	0.122	6.47	Toluene	n. a.	25	187.27	[31]
SBA-15 C	496	0.45	0.083	3.82	Toluene	n. a.	25	415.39	[31]
SBA-15 D	644	0.81	0.094	7.72	Toluene	n. a.	25	321.58	[31]
MCM-41	539	0.64	-	2.43	Toluene	n. a.	25	151.95	[31]

*n. a.: not available data; * equilibrium adsorption capacity extracted from isotherm data; D_{meso}: mesopore diameter*

Table 2. Summary of BTEX adsorption studies on HKUST-1.

Reference	S_{BET} (m^2/g)	V_{total} (mL/g)	V_{micro} (mL/g)	Pore diameter (Å)	Compound	Concentration (ppm)	Temperature (°C)	Adsorption Capacity (mg/g ads)
This work	1733	0.89	0.68	5.4 and 6.9	Toluene	100	23	7
[26]	1122.4	0.47	n. a.	7.5	Toluene	2.5	23	238
[26]	1122.4	0.47	n. a.	7.5	o-xylene	2.5	23	147
[27]	1237	0.47	n. a.	10.51	Toluene	99	25	150
[32]	907.2	0.46	n. a.	n.a.	Toluene	920000	25	516*
[33]	1718	0.68	n. a.	n. a.	o-xylene	5925	125	297*
[33]	1718	0.68	n. a.	n. a.	m-xylene	5925	125	255*
[33]	1718	0.68	n. a.	n. a.	p-xylene	5925	125	297*
[34]	1188.3	0.77	0.41	n. a.	Toluene	950000	25	571*
[35]	1568.5	0.75	0.61	6.51 and 8.25	Benzene	64187	15	794*

*n. a.: not available data; * equilibrium adsorption capacity extracted from isotherm data*

On the other hand, a considerable number of compounds (pollutants) with different polarities and molecular sizes are commonly coexisting in real environments [36], which may lead to competitive adsorption on available adsorption sites, thus resulting in preferential adsorption. Therefore, the study of multicomponent adsorption is a crucial issue to take into account when a material is assessed for pollutant removal or gas analysis. In this sense, only few studies have simulated the adsorption of gas mixtures including BTEX [26], [33], [37].

In this work, three commercially available materials differing in their composition, porosity and surface chemistry have been selected to perform single and multicomponent adsorption of low concentrated BTEX mixtures (10 - 100 ppm). Carbopack® B is a non-porous graphitised carbon black traditionally used as a reference material in sorbent tubes for environmental monitoring [38], [39] and preconcentration devices [40]–[42]. SBA-16 is a mesoporous silica with relatively high specific surface area employed especially in catalytic applications [43, p. 16], [44], [45] and, to a lesser extent, in gas analysis [46]–[48]. Finally, HKUST-1 ($Cu_3(BTC)_2$) is a microporous MOF formed by copper nodes with 1,3,5-benzenetricarboxylic acid linkers between them. This material has been widely employed in catalysis [49], [50], gas analysis [51] as well as in VOC adsorption [52], [53]. These three adsorbents were characterized and evaluated in terms of adsorption capacity in single and multicomponent dynamic adsorption experiments. Furthermore, toluene desorption activation energy was determined and compared between the three materials. The present study provides, therefore, new experimental data concerning the multicomponent adsorption of low concentrated BTEX mixtures, highlighting the importance of adsorbate-adsorbent interactions on the competitive adsorption of aromatics compounds.

2. MATERIALS AND METHODS

2.1 Materials

Commercially available Carbopack® B (60-80 mesh, SUPELCO), HKUST-1 (Basolite® C300, Sigma-Aldrich), and SBA-16 (ACS Materials) were used as received for adsorption tests. Toluene diluted in synthetic air (100 ppm, Air Products, France) and BTEX mixture diluted in nitrogen (10 ppm,

Air Products, France) were employed in temperature programmed desorption (TPD) and dynamic adsorption experiments.

2.2 Characterization of adsorbents

X-ray diffraction patterns were recorded on a Bruker D8 Advance diffractometer, with a Ni detector side filtered Cu Kα radiation (1.5406 Å) over a 2θ range of 5-60°.

Scanning electron microscopy (SEM) images were acquired in a ZEISS GEMINI SEM 500 microscope using an electron high tension (EHT) voltage ranging from 2 to 6 kV.

The textural properties were analysed by means of nitrogen physisorption using a Micromeritics ASAP 2420 equipment. Prior to analysis, the samples were outgassed at 180 °C for 5 h under vacuum. The specific surface area was calculated using the Brunauer–Emmett–Teller (BET) method. The total pore volume was estimated by the single point method from the amount of adsorbed N_2 at a relative pressure (P/P_0) of 0.99. Pore size distributions (PSD) were determined using Barrett, Joyner, and Halenda (BJH) method from the adsorption branch of the isotherm. The micropore volume and micropore surface area were calculated by a t-plot method. Micropore size distribution was calculated by Saito and Foley method [54].

Thermogravimetric analyses (ATG) were performed in a thermobalance coupled with a differential scanning calorimetry apparatus (SDT 650, TA Instruments). The samples were analysed in inert (N_2) atmosphere from room temperature to 500°C by using a 10 K/min heating rate.

Temperature Programmed Desorption (TPD) experiments were used to calculate the toluene desorption energy from the adsorbent surfaces. TPD analyses were carried out in a Micromeritics AutoChem II 2920 equipped with a TCD detector. Samples were outgassed *in-situ* at 280 °C during 1 h. Afterwards, they were cooled down to room temperature and a gas stream of 50 mL/min of toluene diluted in synthetic air (100 ppm, Air Products, USA) was passed through the adsorbent bed for 15 min. Subsequently, samples were analysed using a helium flow rate of 30 mL/min at several temperature

ramps between 10 and 30 K/min for Carbopack® B and SBA-16. Lower heating rates from 4 to 12 K/min were used on HKUST-1 samples to prevent adsorbent decomposition before toluene desorption.

2.3 Dynamic adsorption experiments

Carbopack® B, SBA-16 and HKUST-1 (15 mg) were packed separately in thermal desorption tubes (Sigma Aldrich, USA) using two glass wool plugs. Prior to analysis, the samples were conditioned for 2 h at 280 °C under a helium flow of 50 mL/min using thermal desorber (TurboMatrix 350, Perkin Elmer, USA) in order to ensure a clean surface. Then, the tubes were mounted on a self-made experimental device showed in Figure S1 (Supporting Information). For a single component breakthrough test, toluene diluted in synthetic air (100 ppm, Air Products, France) was flowed through each tube under ambient conditions (room temperature, T=23 °C ± 2 °C). As for the multicomponent adsorption, BTEX mixture diluted in nitrogen (10 ppm, Air Products, France) was employed and flowed at the same temperature, with a 5 mL/min flow rate in both experiments (Mass flow controller 1). The effluent gas stream was continuously analysed by a gas chromatograph (μBTEX-1 In'Air Solutions, France). Before the analysis and in order to avoid the detector saturation, the effluent was diluted using a second mass flow controller operating at 995 mL/min and 95 mL/min nitrogen flow (99.999% purity, Messer, Gemany) for single and multicomponent experiments, respectively, to obtain a concentration of 500 ppb at the analytical instrument inlet. Prior to each adsorption experiment, the peak area corresponding to the initial concentration (C_0) was measured. To this purpose, the gas stream was flowed through a bypass, diluted and analysed. For a given compound, the obtained bypass peak area was used as reference to determine the time at which the adsorbent saturation is reached ($C = C_0$).

The dynamic adsorption capacity (q) for given concentration and flow rate can be calculated as the area above the breakthrough curve using the following equation:

$$q = \frac{F\,C_0}{m}\int_{t_0}^{t_s}\left(1-\frac{C}{C_0}\right)\,dt \qquad (1)$$

where q is the dynamic adsorption capacity per gram of adsorbent (mg/g ads), F is the volume gas flow rate ($m^3\ min^{-1}$), m is the mass of adsorbent (g), t_0 is the initial time (min), t_s is the saturation time (min), C_0 is the initial concentration (mg m^{-3}), C is the outlet concentration (mg m^{-3}) at a given time.

3. RESULTS AND DISCUSSION

3.1 Characterization of the adsorbents

XRD analysis of commercial adsorbents was carried out to assess the crystal structure (Figure 1). Briefly, Carbopack® B exhibits the characteristic diffractions of graphitic carbon (ICDD #00-023-0064), HKUST-1 corresponds to those of $C_{10}H_{10}N_8Zn$ composite (ICDD #00-023-1971) while a broad peak is observed in the case of SBA-16, which is ascribed to amorphous silica, usually appearing in the XRD patterns of ordered mesoporous silicas. Related to the latter, the highest diffractions are observed at small angles, not detectable with the present method. Nevertheless, XRD profiles allow confirming the existing phases.

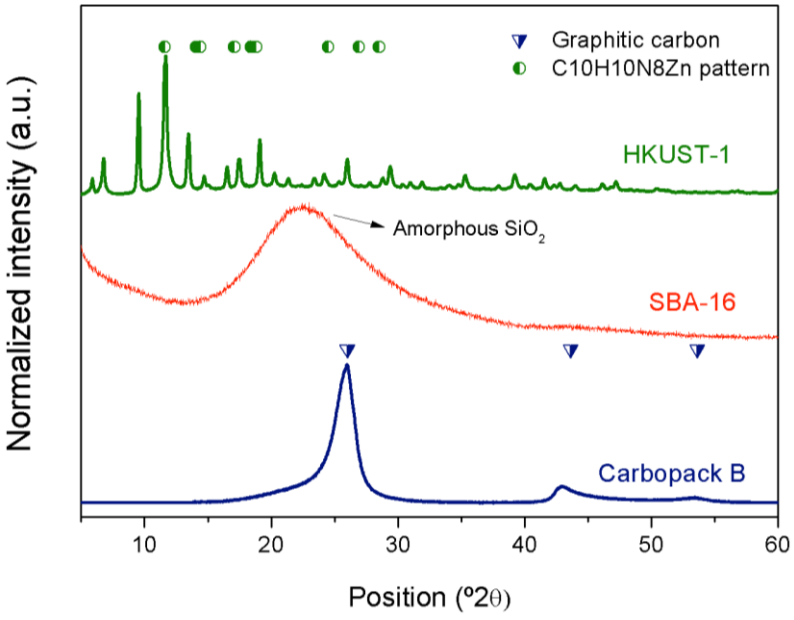

Figure 1. X-Ray diffraction patterns of commercial adsorbents.

Representative SEM micrographs of the studied materials are shown in Figure 2. Both Carbopack® B and SBA-16 samples (Figs. 2a and 2b, respectively) are characterized by different sized agglomerates (ranging from 10 to 180 µm) with highly grainy surface. In contrast, HKUST-1 (Fig. 2c) exhibits a homogeneous morphology constituted by smooth surface octahedral crystals having uniform sizes between 10 and 25 µm. The latter is congruent with previous literature reports [26], [35], [55], [56] or was purchased as commercial material [57].

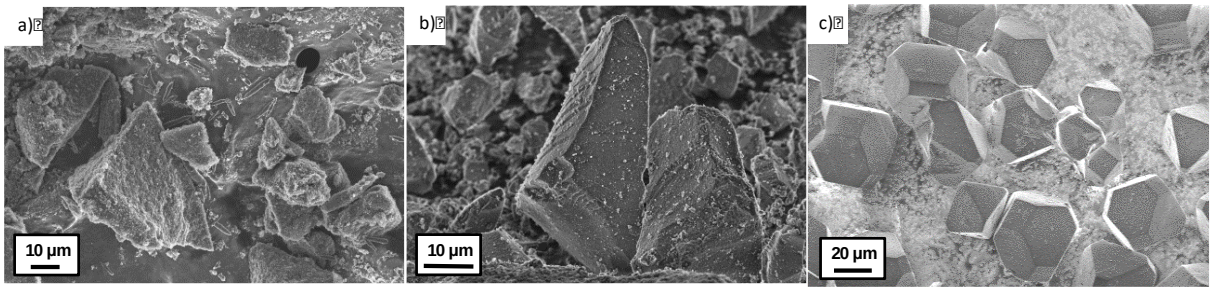

Figure 2. SEM micrographs of (a) Carbopack® B, (b) SBA-16 and (c) HKUST-1

The corresponding N_2 adsorption-desorption isotherms are presented in Figure 3. Carbopack® B (Fig. 3a) exhibits a type III isotherm according to the IUPAC classification, which is characteristic of non-porous materials. The significant increase in adsorbed N_2 observed at P/P_0 = 0.8-0.95 suggests that, at this point, all the layers were saturated, and the adsorbate molecules are filling the interparticle space. Thus, the estimated total pore volume may not correspond only to the pores present on the adsorbent but also to the space between particles. As displayed in Fig. 3b, SBA-16 exhibits a type IV isotherm, characteristic of mesoporous materials. A hysteresis loop can be noticed at intermediate P/P_0 associated to capillary condensation occurring in mesopores [58]. The form of the hysteresis curve, with two different widths, reveals the presence of two different types of pores. This evidence was confirmed by the pore size distribution (see Fig. S2) with pore diameters of nearly 3.4 and 6.0 nm. The high quantity absorbed by HKUST-1 at low pressures (Fig. 3c) followed by a long horizontal plateau at higher pressures is typical of type I adsorption isotherms and can be associated to a very strong adsorption

within the micropores [37], [56], [59]. Most probable pore diameter were determined by Saito and Foley method (see Figure S3) resulting to be 5.4 and 6.9 Å, similar to the diameters of the small (4.5 Å) and large cages (9 Å) theoretically presented in the MOF structure [53]. These diameters imply that, although the dynamic diameters of BTEX molecules are larger (from 0.59 to 0.68 nm; see Table S1) than the size of the small cages, they may enter inside the larger pores thus interacting by means of π-π stacking with the organic linkers.

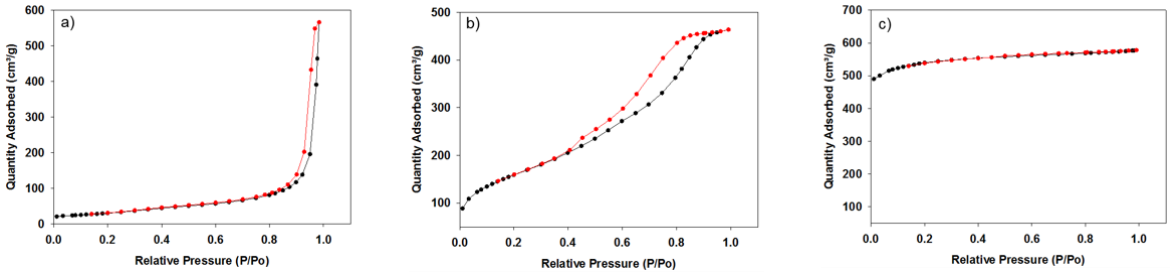

Figure 3. Nitrogen adsorption (black) and desorption (red) isotherms at 77 K of (a) Carbopack® B, (b) SBA-16, (c) HKUST-1

The textural properties of all studied samples are summarized in Table 3. As expected, the specific surface area increases with the porosity (112, 572, 1734 $m^2\ g^{-1}$ for Carbopack® B, SBA-16 and HKUST-1, respectively) with the highest value for the microporous adsorbent. Concerning the pore volume, SBA-16 presents a total volume of 0.72 $cm^3\ g^{-1}$, barely lower than that observed for HKUST-1, 0.89 $cm^3\ g^{-1}$. These adsorbents exhibit therefore similar pore volumes but different pore diameters. According to the pore size distribution, 95% of the total pore volume in SBA-16 corresponds to pores having 3.4 or 6.0 nm diameter (V_{meso}). In contrast, most of the pores in HKUST-1 have diameters around 0.54 and 0.69 nm. The micropore volume of HKUST-1 sample was calculated to be 0.68 $cm^3\ g^{-1}$ which corresponds to 77% of the total volume, thus assessing a highly microporous nature.

Table 3. Textural properties of investigated adsorbents

Sample	S_{BET} ($m^2\ g^{-1}$)	V_{total} ($cm^3\ g^{-1}$)	V_{meso} ($cm^3\ g^{-1}$)	V_{micro} ($cm^3\ g^{-1}$)	D_{pore} (nm)
Carbopack® B	112	-	-	-	-
SBA-16	572	0.72	0.68	-	3.4/6.0
HKUST-1	1733	0.89	0.14	0.68	0.54/0.69

S_{BET}: BET surface area; V_{total}: total pore volume; V_{meso}: mesoporous volume; V_{micro}: microporous volume; D_{pore}: pore diameter.

In order to evaluate both the thermal stability and water affinity of the adsorbents, a thermogravimetric study was carried out over the samples after 2 h of exposure to ambient air (Figure S4). All samples have in common a first weight loss situated around 100 °C, usually ascribed to physisorbed water. As deduced from the thermal profiles, Carbopack B is the most hydrophobic adsorbent (showing less than 2% weight loss at 100°C) followed by SBA-16 (6%) and HKUST-1 (exhibiting 32% weight loss between 80 and 150°C). It is well known from the literature that HKUST-1 exhibits a high affinity towards water [26], [35], [55] since water molecules can coordinate to the free copper sites [60]. These results are in agreement with those observed by Seo *et al.* [61] reporting a weight loss of 30% at ~110°C associated to a presumed loss of 15 water molecules (29.7%) per Cu_3 unit present in HKUST-1 structure. This great affinity to water prevents the use of HKUST-1 as an effective adsorbent in moist environments since water molecules may occupy adsorption sites resulting in a considerable decrease in the adsorption capacity. Nevertheless, this adsorbent can be employed for VOC removal in dry environments such as aircraft cabins where the relative humidity ranges between 2 and 23% [62].

HKUST-1 decomposition takes place at around 320°C as evidenced by a dramatic weight loss of ~30% accompanied by a heat release (exothermic peak), which is usually ascribed to the MOF decomposition into Cu_2O and CuO [55], [61] and the subsequent benzene di-carboxylic group oxidation [63]. The material decomposition involves the loss of its chemical structure and, thus, its adsorption properties. Consequently, this temperature must not be exceeded during the activation/desorption process. No remarkable thermal events were observed at higher temperatures. As depicted in Figure S4a

and S4b, Carbopack® B and SBA-16 suffered a total weight loss of 3 and 7%, respectively, up to 400°C, demonstrating high thermal stability.

3.2 Single component adsorption experiments

Single aromatic adsorption experiments were carried out using toluene as probe molecule (Figure 4). The breakthrough curves represent the evolution of the pollutant concentration in the effluent leaving the adsorbent bed as a function of time. They provide information about the bed adsorption capacity and the kinetics of the adsorption process. Three different zones can be distinguished in these consecutive curves: the unsaturated zone, mass transfer zone and saturated zone. The first zone ranges from the beginning of the experiment (t_0) to the breakthrough time (t_b). Usually, in air treatment, even a very low amount of pollutant in the effluent is not allowable; therefore, the breakthrough time is reached when 5% of the concentration of the feed (C_0) is leaving the adsorbent bed. Prior to the breakthrough, adsorption can be considered complete. Industrially, the quantity of pollutant adsorbed during this stage represents the usable capacity of the reactor. From the breakthrough point, the concentration measured at the outlet progressively increases until the saturation time (t_s) is reached ($C/C_0 = 1$). The steepness of the concentration profile between t_b and t_s represents the mass transfer zone. The profile of this zone provides insights about the mass transfer from gas phase to the adsorption sites inside the sorbent particles. From an industrial point of view, a short mass transfer zone is preferred considering that from t_b the adsorption is considered ineffective. From t_s, all the adsorption sites are occupied, and no further adsorption takes place. Therefore, the measured concentration of the effluent at the outlet is equal to the concentration of the feed. At this point, the dynamic adsorption capacity of the adsorbent under the operating conditions can be determined.

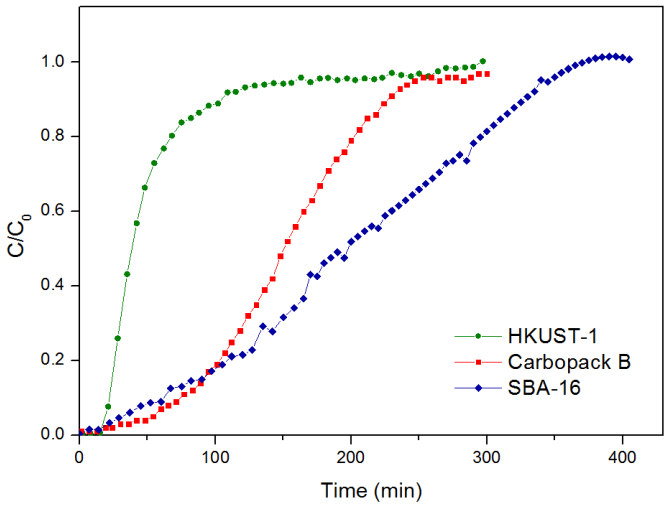

Figure 4. Breakthrough curves of toluene over SBA-16 (blue), Carbopack® B (red) and HKUST-1 (green). Toluene concentration = 100 ppm, flow rate 5 mL/min.

Table 4 shows the obtained breakthrough times and the calculated dynamic adsorption capacities. Although the duration of the unsaturated zone is similar for the three adsorbents, HKUST-1 exhibits the shortest breakthrough time. It could be somehow related with the adsorbent density, which is different in each case. Certainly, HKUST-1 density (bulk density of 0.35 g/cm^3) was higher compared to Carbopack® B and SBA-16, which implies that the adsorbent bed length was slightly shorter and, thus, toluene molecules might pass through faster.

As evidenced by the breakthrough curves, the mass transfer zones have different shapes depending on the adsorbent, being the steepness of the concentration front related to the kinetics of the adsorption process. In this way, the breakthrough curve of HKUST-1 increases sharply from the breakthrough point to the saturation suggesting fast toluene adsorption kinetics. It might be related both to the particle size, as smaller sizes should enable higher intraparticle mass transfer rates, and with the presence of micropores. HKUST-1 consists of smaller particles (10 – 25 µm, see Fig. 2), compared with the other two adsorbents (10 – 180 µm), which may lead to shorten the mass transfer zone.

Table 4. Breakthrough times and adsorption capacities obtained in toluene adsorption experiments

Adsorbent	Breakthrough time (min)	Adsorption Capacity (mg/ g ads)
Carbopack® B	54	18.74
SBA-16	32	24.87
HKUST-1	20	6.96

The adsorbent adsorption capacities were calculated from the area below the respective breakthrough curves (Fig.4). Surprisingly, the adsorbent with higher specific surface area (HKUST-1) led to the lowest adsorption capacity, suggesting that toluene adsorption may be influenced by different factors. Theoretically, in HKUST-1, the structure is composed by two large cages with a pore diameter of 9 Å and internal diameters of 13.2 and 11.1 Å connected to 6 Å sized smaller cages with 4.5 Å diameter. These values are slightly different from those obtained experimentally (5.4 and 6.9 Å), however, in both cases, toluene molecules (kinetic diameter = 5.8 Å) are not expected to enter in the smaller cages, but they can be adsorbed in the larger ones. Nevertheless, if HKUST-1 is slightly hydrated, the water molecules may reduce the opening diameter of pores thus preventing the entrance of toluene molecules [26], [64]. Despite the existence of adsorbed water molecules is highly unlikely after the adsorbent outgassing at 280 °C, it has been demonstrated that the powder pre-treatment at temperatures above 250 °C may cause a drastic decrease in porosity [53], hence reducing the available surface area.

In contrast to HKUST-1, SBA-16 presents the highest adsorption capacity compared to other adsorbents. The results suggest that the presence of large pores (3.4 - 6.0 nm) can lead to an increase in the adsorption capacity, as demonstrated by Zhang *et al.* for the toluene adsorption over UiO-66 MOF [65]. They reported an enhancement of toluene dynamic adsorption capacity of the micro-mesoporous UiO-66 compared to the microporous counterpart, due to an increase in the molecular transfer rate that allows toluene molecules to diffuse in the material further thus increasing the residence time of the adsorbate molecules in the adsorbent bed. Moreover, it seems that the adsorption of toluene molecules in larger pores can promote the adsorption of new toluene molecules by π-π stacking within the mesopores, which may lead to higher adsorption capacity. Carbopack® B exhibited lower adsorption

capacity than SBA-16 probably due to its lower specific surface area and, thus, less available adsorption sites.

Comparison with the literature

The adsorption of aromatics has been widely studied in the last years. However, the variability of the conditions used in the experiments render difficult the comparison of the results. Table 2 summarizes the results for aromatics adsorption previously reported over HKUST-1 [26], [27], [32]–[35]. Since most of the studies were performed at very high concentrations (5925 - 950000 ppm) compared to ours (10 ppm), the measured adsorption capacities in these studies were (in comparison) rather high. Only the results reported by Vellingiri *et al.* [27] were conducted under similar conditions (initial concentration of 99 ppm and 25 °C) and can be compared to the adsorption capacity determined herein. In this regard, our measured toluene adsorption capacity over HKUST-1 sample (6.96 mg/g) was significantly lower than the value of 150 mg/g obtained by Vellingiri et *al*. The difference could be associated to the temperature employed during the outgassing process, 170 °C (Vellingiri et *al*.) instead of 280 °C (this study), which would further confirm that HKUST-1 is very sensitive to the temperature, starting its structural degradation at T < 280 °C.

Similarly, Table 1 summarizes the obtained results for both benzene and toluene adsorption over micro- and mesoporous silicas. As noted above, most of the experiments were conducted at very high initial concentrations, which do not provide representative data for realistic environments. Mesoporous silicas with diverse structures have been tested for aromatics adsorption, some of them combining meso- and micropores. The latter ones exhibited higher adsorption performance due to the stronger interactions of the molecules in the narrow pores that promotes their adsorption. Indeed, considering only the mesoporous silicas, the pore volume did not seem to be a key parameter influencing the adsorption, whilst a linear increase in adsorption capacity appears to be related to the decrease in the pore diameter, as shown in Figure S5 for toluene. This may explain the low toluene adsorption capacity of SBA-16 compared to other silicas with narrower mesopores.

As for graphitised carbon blacks solids, few data addressing BTEX total adsorption capacity have been found in literature. In contrast, these materials have been traditionally used for VOC sampling; the studies dealing mainly with its regeneration [40], uptake rates [39] and samples stability [66]. Furthermore, Carbopack® B has been lately replaced by Carbopack® X due to its higher specific surface area (240 m^2/g to be compared with 112 m^2/g for Carbopack® B). The adsorption capacity of this material was investigated by Khan *et al.* that reported a benzene adsorption capacity of 6.79 mg/g (50 ppm, 25 °C) [67]. This value, relatively lower than the toluene adsorption capacity found for Carbopack® B in the present work, could be explained by the lower volatility of toluene, as it will be highlighted during the multicomponent experiments.

3.3 Multicomponent adsorption experiments

Single component adsorption experiments allowed determining the adsorption capacity of each material, illustrating the differences on toluene adsorption among them. In indoor air, however, a broad spectrum of gaseous pollutants usually coexists, resulting in competitive adsorption phenomena. Therefore, the capacity of an adsorbent for pollutant removal or analysis cannot be based solely on the adsorption of a single compound. To determine this capacity in a more realistic environment, a mixture of aromatic compounds was employed for dynamic adsorption experiments.

Figure 5 illustrates the obtained breakthrough curves for BTEX under ambient conditions (T=296 K ± 2 K), using a feed of 5 mL/min containing 10 ppm of each pollutant. For each adsorbent, the plot is composed of five breakthrough curves corresponding to each single compound in the mixture, excepting coeluted m- and p-xylenes that are represented by the same curve. In general, the obtained plots are somewhat comparable, and higher boiling point compounds are preferentially adsorbed following the order benzene > toluene > ethylbenzene > m/p-xylenes > o-xylene. Nevertheless, the concentration profiles and the calculated adsorption capacities (see Table 5) for each compound vary from one adsorbent to another suggesting that slightly different adsorbate-adsorbent interactions/diffusional processes are co-existing.

Initially, all compounds were completely adsorbed, excepting benzene over Carbopack® B that passed through the adsorbent bed from the beginning. Afterwards, the other species start to break through in accordance with their increasing boiling point. In this way, the outlet adsorbate concentrations start to rise, reaching, in the case of benzene and toluene, higher values than the inlet concentration ($C/C_0 > 1$). This phenomenon, called roll-up, appears when the thermodynamic effects govern the adsorption process [68] *i.e.* the adsorbate with weaker interactions is replaced by other species with more favourable adsorbate-adsorbent interactions. Roll-up was observed over all materials in different degrees, resulting in the desorption of the most volatile compounds in favour of the adsorption of the less volatile compounds.

SBA-16 and Carbopack® B present minimum benzene/toluene roll-up whereas over HKUST-1 the effect is more pronounced. Consequently, the adsorption capacities of each compound were strongly related to adsorbate-adsorbent interactions as well as to the presence of micropores.

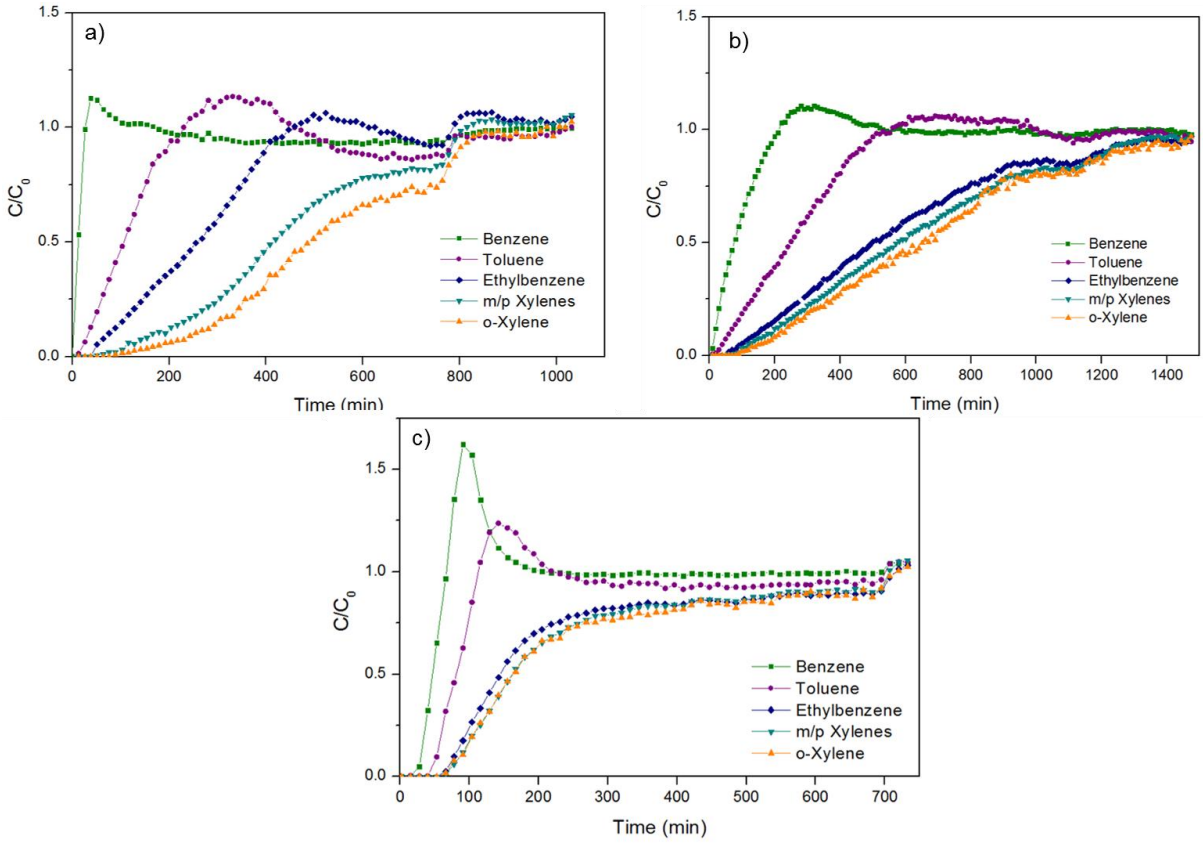

Figure 5. Breakthrough curves for BTEX over Carbopack® B (a), SBA-16 (b), and HKUST-1 (c). BTEX concentration = 10 ppm, flow rate 5 mL/min.

In Carbopack® B, London interactions are the prevailing adsorbate-adsorbent forces that govern the adsorption process due to the non-polar surface of this material. Consequently, the adsorption capacity for each compound is considerably different due to the different strength of these interactions and, logically, follows the order of the boiling points (o-xylene > m/p-xylenes > ethylbenzene > toluene > benzene) provided in Table S1. It should be noted that the effect of the competitive sorption between the different species in this material is remarkable, resulting in the total desorption of the most volatile compound, *i.e*. benzene. Therefore, special attention should be paid when this material is used to remove/analyze benzene or similar boiling points pollutants in presence of less volatile compounds.

Even when interactions of different nature can be established, London forces are usually the driving force in the adsorption of high boiling point molecules, having also high molecular mass. It is known from the literature that in mesoporous silicas, the hydroxyl groups located at the surface may behave as weak acid sites interacting with the π-electrons of the aromatic rings [69], [70]. Hence, in SBA-16, adsorption can take place via London forces and weak π-system−hydrogen bonding of the aromatic ring with silanols. For these dipole forces, the strength increases with the polarizability of the molecule, which explains the low adsorption capacity obtained for benzene and toluene compared to ethylbenzene and m/p-xylenes. As in the previous case, the adsorption capacity follows the order of the boiling points (o-xylene > m/p-xylenes > ethylbenzene > toluene > benzene). Obviously, o-xylene, with its highest boiling point and high polarizability, demonstrated the highest adsorption capacity.

Similarly to SBA-16, BTEX adsorption in HKUST-1 occurs through London forces as well as π-interactions but, in this case, these interactions are between the aromatic ring of the adsorbate and those presented in the HKUST-1 structure [71] formed with benzene 1,3,5-tricarboxylate linkers. Once again, the adsorption capacity follows the order: o-xylene > m/p-xylenes > ethylbenzene > toluene > benzene. However, the roll-up observed in the breakthrough curve for benzene and toluene is considerably more pronounced than in the mesoporous silica. This difference is probably due to the fact that in HKUST-1, BTEX molecules are adsorbed within the micropores instead of mesopores, and the BTEX molecules size is very close to that of micropores. Since London forces are distance sensitive,

they are expected to play an important role in the adsorption within the micropores resulting in a huge difference between the adsorption capacities of smaller molecules, *i.e.* benzene and toluene, compared to the larger molecules.

These results are in line with those reported in other studies. Chevalier *et al*. performed breakthrough experiments of 1.25 ppm binary mixtures of toluene and o-xylene on HKUST-1 [26]. They observed a pronounced roll-up effect of toluene indicating highly selective adsorption of o-xylene over toluene. Peralta *et al*. investigated the single and competitive adsorption of xylene isomers on HKUST-1 [33]. In single experiments, they found similar adsorption capacities for the three isomers, with a slightly higher value for o-xylene. Nevertheless, in multicomponent experiments, a preferential adsorption of o-xylene over m- and p-xylenes was reported.

As *a priori* expected, the results regarding total adsorption capacity in the multicomponent adsorption study are consistent with those obtained in single component experiments. Total adsorption capacity followed the order SBA-16 > Carbopack® B > HKUST-1. It is clear from our results that multicomponent adsorption is a complex process in which polarizability, molecular size, surface chemistry and porosity play a crucial role. In this context, the multicomponent breakthrough curves can provide valuable information about the key aspects in competitive adsorption of pollutants according to their characteristics. SBA-16 has demonstrated the highest adsorption capacity for aromatics in both single and multicomponent experiments. Moreover, among the investigated materials, the mesoporous silica exhibited the minimum roll-up, thus avoiding the release of compounds previously adsorbed, which can be dangerous since benzene is the most hazardous one. Therefore, SBA-16 can be a promising candidate for applications to pollutant removal and analysis. Nevertheless, for its use in absorbers at industrial scale, enough length should be expected to prevent early breakthroughs.

Table 5. Breakthrough times and adsorption capacities obtained in multicomponent adsorption experiments

	Breakthrough time (min)			Adsorption Capacity (mg/ g ads)		
Compound	**CB**	**SB**	**HK**	**CB**	**SB**	**HK**
Benzene	1	11	28	0	0.6	0.16
Toluene	23	40	44	1.47	2.81	0.82
Ethylbenzene	51	99	70	3.31	8.16	3.25
m/p - Xylenes	116	129	76	6.13	8.96	3.45
o - Xylene	190	159	73	7.32	9.67	3.59
Total	-	-	-	18.22	30.2	11.28

CB: Carbopack® B; SB: SBA-16; HK: HKUST-1

3.4 Desorption activation energy of toluene

In gas analysis as well as in pollutant removal, the activation energy of the desorption process of contaminants is a crucial parameter for a sound selection of an adsorbent. This energy should be relatively high to enable the trapping of pollutants at room temperature but low enough to permit its desorption at moderate temperatures, typically in the range 150 – 350 °C. In this context, TPD is powerful surface analysis technique providing valuable information regarding desorption kinetics, reaction order or desorption activation energy, as well as the variation of each of these factors with respect to the adsorbate coverage [72].

In this work, toluene TPD experiments were carried out at different heating rates, between 10 to 30 K/min, over Carbopack® B and SBA-16 samples. Lower heating rates from 4 to 12 K/min were used over HKUST-1 to prevent adsorbent decomposition before toluene desorption. The obtained desorption curves are displayed in Fig. 6.

Whatever the adsorbent, only one desorption peak was detected, thus indicating that the adsorption of toluene took place from a single adsorption site. As illustrated in Fig. 6, an increment in the heating rate led to an increase in the peak desorption temperature (T_p). SBA-16 and Carbopack® B exhibited similar desorption temperatures at the same heating rates, whilst higher temperatures were required for HKUST-1. This implies that higher energies are required to desorb toluene from this

material and, consequently, either the toluene-adsorbent interactions are stronger or the diffusional limitations higher compared to those of SBA-16 and Carbopack® B. Relating this to the obtained results during the competitive adsorption experiments, where toluene was released from HKUST-1 (Fig. 5c), it might be expected that the adsorbate-adsorbent interactions of C8 aromatics could be even stronger.

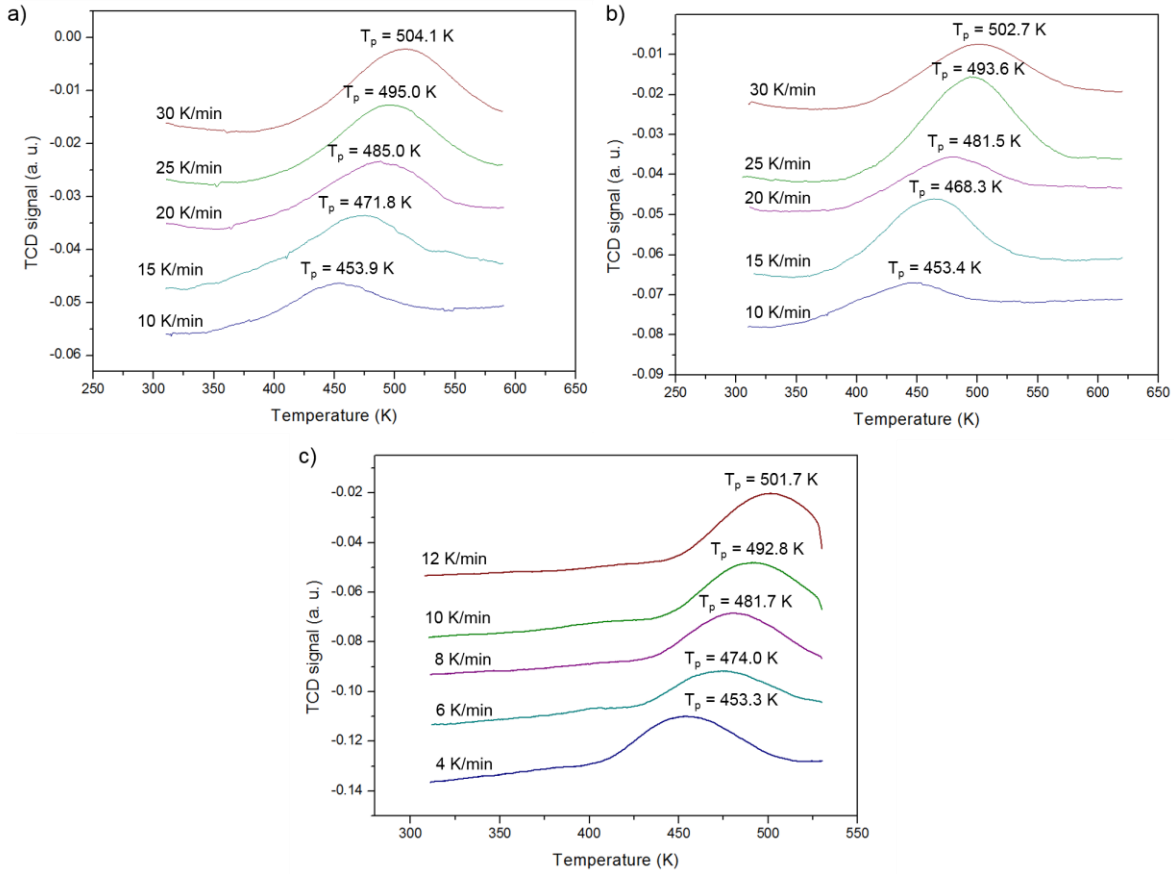

Figure 6. Toluene desorption TPD curves over Carbopack® B (a), SBA-16 (b) and HKUST-1 (c) samples at different heating rates.

The desorption activation energy (E_d) of toluene can be estimated using the data from TPD experiments [71], [72], [73] according to the Polanyi–Wigner equation [76]:

$$-\frac{d\theta}{dT} = \frac{A}{\beta}\theta^n \exp\left(-E_d/RT\right) \quad (2)$$

where θ is the surface coverage, T (K) is the temperature, A (s^{-1}) is the desorption rate coefficient, β (K s^{-1}) is the heating rate, n is the order of the reaction, E_d (J mol^{-1}) is the activation energy of the

desorption and R (J mol^{-1} K^{-1}) is the ideal gas constant. During the desorption, the desorption peak temperature T_p is reached when $\frac{d^2\theta}{dT^2} = 0$. Taking this into account and assuming that desorption follows first order kinetics, Eq. ((2) yields:

$$\ln(\frac{RT_p^2}{\beta}) = \ln\left(\frac{E_d}{A}\right) + \frac{E_d}{RT_p} \quad (3)$$

In this way, by plotting $\ln(\frac{RT_p^2}{\beta})$ versus $1/T_p$, the toluene desorption activation energy over the different materials can be calculated (Fig. 7). The obtained desorption activation energies are 33.7, 33.8 and 35.9 kJ/mol for SBA-16, Carbopack® B and HKUST-1, respectively. These values are very close, indicating that the strength of the adsorbate-adsorbent interactions is similar in all investigated materials. Among them, HKUST-1 exhibited a barely higher desorption activation energy probably due to both the stronger toluene electrostatic interactions within the micropores and the expected lower diffusional coefficient. In addition, the presence of benzyl groups in HKUST-1 structure allows forming π-π interactions with toluene, hence enhancing the energy required for the desorption. In the case of mesoporous and non-porous materials such as SBA-16 and Carbopack® B, the molecule diffusion should not be limited, thus leading to a lower desorption activation energy. Nevertheless, the activation energy was found to be almost identical on SBA-16 and Carbopack® B, suggesting that the presence of pores much larger than the size of the adsorbate molecule did not significantly influence the adsorbate-adsorbent interactions.

The activation energy of the desorption process was 35.9 kJ/mol for HKUST-1, being barely lower than 43.8 kJ/mol reported by Xu et al. [75] for toluene and slightly higher than the value of 33.8 kJ/mol determined by Zhao *et al*. for the desorption of benzene [35]. This difference might be mostly related to the lower benzene cross-sectional area, which allows a better diffusion within the micropores.

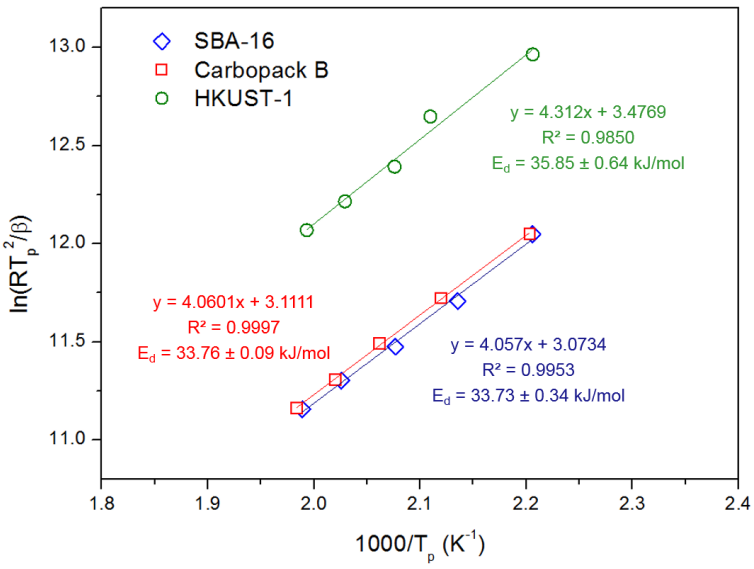

Figure 7. Linear dependence between ln (RT^2_p/β) and $1/T_p$ for TPD of toluene on SBA-16 (blue), Carbopack® B (red) and HKUST-1 (green). The desorption activation energies are derived from the slope according to Eq. (3).

From an industrial point of view, a lower desorption energy is preferred since less energy is required for the adsorbent regeneration, thus resulting in more cost-effective processes. Therefore, considering only the energy aspect, SBA-16 seems again to be the best candidate for pollutant removal and analysis among the studied adsorbents.

4. CONCLUSIONS

In this study, three commercial adsorbents with different porosities and surface chemistries were characterized and their BTEX adsorption was assessed in terms of breakthrough time and adsorption capacity. Firstly, single component dynamic adsorption studies were carried out using toluene as a probe molecule. Those results suggest that breakthrough time is closely related to both particle size, being shorter for smaller particles, and the micropores presence. From the breakthrough curves, adsorption capacity values of those materials were calculated to be 18.7, 24.9 and 7.0 mg/g for Carbopack® B, SBA-16 and HKUST-1, respectively. It was expected to find an increasing adsorption capacity as

specific surface area increases. However, the material with larger specific surface area (HKUST-1) exhibited the lowest adsorption capacity, pointing out possible diffusional limitations related to the microporous structure. The same trend in adsorption capacity was found during multicomponent adsorption experiments. Furthermore, roll up effect was observed to some extent with all adsorbents. The intensity of this phenomenon was related to adsorbate-adsorbent interactions in each case, indicating that the strength of these interactions plays a major role in competitive adsorption. Roll-up effect is of great importance when using adsorbents in air treatment, since hazardous compounds can be released even when the adsorbent is far from saturation. Finally, the activation energy for toluene desorption determined by TPD technique was 33.8, 33.7 and 35.9 kJ/mol for Carbopack® B, SBA-16 and HKUST-1, respectively. The microporous material (HKUST-1) exhibited the highest desorption activation energy due most probably to both stronger molecule interactions and diffusional limitations within the micropores. Non-porous (Carbopack® B) and mesoporous solids (SBA-16) exhibited almost identical energies suggesting comparable adsorbate-adsorbent interactions and diffusional coefficients. Among the investigated adsorbents, SBA-16 seems to be the most appropriate for air treatment due to its superior adsorption capacity, minimal roll-up and low desorption temperature. Nevertheless, a detailed study of the adsorption capacity of this material after several regeneration cycles should be performed to fully evaluate its suitability for air treatment and gas analysis.

Acknowledgements

This work has received funding from the Clean Sky 2 Joint Undertaking under the European Union's Horizon 2020 research and innovation program under grant agreement No. 687014 (MACAO project) and under the Marie Skłodowska-Curie Grant Agreement No. 643095 (MIGRATE project) [H2020-MSCA-ITN-2014]. This project has also been supported by the European Union's through the LIFE SMART IN'AIR – Smart indoor air monitoring network to reduce the impacts of pollutants on environment and health – under grant number LIFE17 ENV/FR/000330.

REFERENCES

[1] I. Lara-Ibeas et al., “BTEX near real-time monitoring in two primary schools in La Rochelle, France,” Air Qual Atmos Health, vol. 11, no. 9, pp. 1091–1107, Nov. 2018.

[2] C. Mandin et al., “Assessment of indoor air quality in office buildings across Europe – The OFFICAIR study,” Science of The Total Environment, vol. 579, pp. 169–178, Feb. 2017.

[3] R. Nasreddine, V. Person, C. A. Serra, C. Schoemaecker, and S. Le Calvé, “Portable novel micro-device for BTEX real-time monitoring: Assessment during a field campaign in a low consumption energy junior high school classroom,” Atmospheric Environment, vol. 126, pp. 211–217, Feb. 2016.

[4] M. Śmiełowska, M. Marć, and B. Zabiegała, “Indoor air quality in public utility environments—a review,” Environ Sci Pollut Res Int, vol. 24, no. 12, pp. 11166–11176, 2017.

[5] R. Montero-Montoya, R. López-Vargas, and O. Arellano-Aguilar, “Volatile Organic Compounds in Air: Sources, Distribution, Exposure and Associated Illnesses in Children,” Annals of Global Health, vol. 84, no. 2, Jul. 2018.

[6] M. Verriele et al., “The MERMAID study: indoor and outdoor average pollutant concentrations in 10 low-energy school buildings in France,” Indoor Air, vol. 26, no. 5, pp. 702–713, Oct. 2016.

[7] A. Kumar and I. Víden, “Volatile Organic Compounds: Sampling Methods and Their Worldwide Profile in Ambient Air,” Environ Monit Assess, vol. 131, no. 1, pp. 301–321, Aug. 2007.

[8] M. P. Tsakas, A. P. Siskos, and P. Siskos, “Indoor Air Pollutants and the Impact on Human Health,” Chemistry, Emission Control, Radioactive Pollution and Indoor Air Quality, Jul. 2011.

[9] F. Ahmed et al., “Impact of household air pollution on human health: source identification and systematic management approach,” SN Appl. Sci., vol. 1, no. 5, p. 418, Apr. 2019.

[10] G. Hoek et al., “Long-term air pollution exposure and cardio- respiratory mortality: a review,” Environmental Health, vol. 12, no. 1, p. 43, May 2013.

[11] B. Guieysse, C. Hort, V. Platel, R. Munoz, M. Ondarts, and S. Revah, “Biological treatment of indoor air for VOC removal: Potential and challenges,” Biotechnology Advances, vol. 26, no. 5, pp. 398–410, Sep. 2008.

[12] G. R. Parmar and N. N. Rao, “Emerging Control Technologies for Volatile Organic Compounds,” Critical Reviews in Environmental Science and Technology, vol. 39, no. 1, pp. 41–78, Dec. 2008.

[13] M. Słomińska, S. Król, and J. Namieśnik, “Removal of BTEX Compounds From Waste Gases; Destruction and Recovery Techniques,” Critical Reviews in Environmental Science and Technology, vol. 43, no. 14, pp. 1417–1445, Jan. 2013.

[14] G. B. Baur, “Development of Adsorbents for Selective Volatile Organic Compounds Removal from Diluted Gas Streams,” Infoscience, 2015. [Online]. Available: https://infoscience.epfl.ch/record/212805. [Accessed: 30-Jun-2019].

[15] K. Zhou et al., “Activated carbons modified by magnesium oxide as highly efficient sorbents for acetone,” RSC Adv., vol. 8, no. 6, pp. 2922–2932, 2018.

[16] A. Khan, S. J. Mandokhail, N. Mohammad, Z. Baloch, M. Siddique, and M. Akram, “Comparative Analysis of Pressure Regions of Gaseous Benzene Using Ground Activated Carbon Sorbents Under Ambient Conditions,” Journal of Applied and Emerging Sciences, vol. 8, no. 2, pp. pp160-167–167, Apr. 2019.

[17] B. Rubahamya, K. S. K. Reddy, A. Prabhu, A. A. Shoaibi, and C. Srinivasakannan, “Porous carbon screening for benzene sorption,” Environmental Progress & Sustainable Energy, vol. 38, no. s1, pp. S93–S99, 2019.

[18] H. Q. A. Le and D. T. Phan, “Investigation of BTEX Adsorption on Carbon Nanotubes Cartridges from Air Samples,” AMM, vol. 889, pp. 216–222, Mar. 2019.

[19] J. Senthilnathan, K.-H. Kim, J.-C. Kim, J.-H. Lee, and H. N. Song, “Indoor Air Pollution, Sorbent Selection, and Analytical Techniques for Volatile Organic Compounds.,” Asian Journal of Atmospheric Environment (AJAE), vol. 12, no. 4, 2018.

[20] J. Wang et al., “Compact prototype microfabricated gas chromatographic analyzer for autonomous determinations of VOC mixtures at typical workplace concentrations,” Microsystems & Nanoengineering, vol. 4, p. 17101, Apr. 2018.

[21] M. Bahri, F. Haghighat, H. Kazemian, and S. Rohani, “A comparative study on metal organic frameworks for indoor environment application: Adsorption evaluation,” Chemical Engineering Journal, vol. 313, pp. 711–723, Apr. 2017.

[22] X. Zhang, Y. Yang, L. Song, J. Chen, Y. Yang, and Y. Wang, “Enhanced adsorption performance of gaseous toluene on defective UiO-66 metal organic framework: Equilibrium and kinetic studies,” Journal of Hazardous Materials, vol. 365, pp. 597–605, Mar. 2019.

[23] L.-H. Xie, X.-M. Liu, T. He, and J.-R. Li, “Metal-Organic Frameworks for the Capture of Trace Aromatic Volatile Organic Compounds,” Chem, vol. 4, no. 8, pp. 1911–1927, Aug. 2018.

[24] C. Liu, L.-Q. Yu, Y.-T. Zhao, and Y.-K. Lv, “Recent advances in metal-organic frameworks for adsorption of common aromatic pollutants,” Microchim Acta, vol. 185, no. 7, p. 342, Jun. 2018.

[25] J. E. Szulejko, K.-H. Kim, and J. Parise, “Seeking the most powerful and practical real-world sorbents for gaseous benzene as a representative volatile organic compound based on performance metrics,” Separation and Purification Technology, vol. 212, pp. 980–985, Apr. 2019.

[26] V. Chevalier, J. Martin, D. Peralta, A. Roussey, and F. Tardif, “Performance of HKUST-1Metal-Organic Framework for a VOCs mixture adsorption at realistic concentrations ranging from 0.5 to 2.5 ppmv under different humidity conditions,” Journal of Environmental Chemical Engineering, p. 103131, Apr. 2019.

[27] K. Vellingiri, P. Kumar, A. Deep, and K.-H. Kim, “Metal-organic frameworks for the adsorption of gaseous toluene under ambient temperature and pressure,” Chemical Engineering Journal, vol. 307, pp. 1116–1126, Jan. 2017.

[28] W. Zhang, Z. Qu, X. Li, Y. Wang, D. Ma, and J. Wu, “Comparison of dynamic adsorption/desorption characteristics of toluene on different porous materials,” Journal of Environmental Sciences, vol. 24, no. 3, pp. 520–528, Mar. 2012.

[29] B. Dou, Q. Hu, J. Li, S. Qiao, and Z. Hao, “Adsorption performance of VOCs in ordered mesoporous silicas with different pore structures and surface chemistry,” Journal of Hazardous Materials, vol. 186, no. 2, pp. 1615–1624, Feb. 2011.

[30] Q. Hu, J. J. Li, Z. P. Hao, L. D. Li, and S. Z. Qiao, “Dynamic adsorption of volatile organic compounds on organofunctionalized SBA-15 materials,” Chemical Engineering Journal, vol. 149, no. 1, pp. 281–288, Jul. 2009.

[31] Y. Qin, Y. Wang, H. Wang, J. Gao, and Z. Qu, “Effect of Morphology and Pore Structure of SBA-15 on Toluene Dynamic Adsorption/Desorption Performance,” Procedia Environmental Sciences, vol. 18, pp. 366–371, Jan. 2013.

[32] F. Xu, S. Xian, Q. Xia, Y. Li, and Z. Li, “Effect of Textural Properties on the Adsorption and Desorption of Toluene on the Metal-Organic Frameworks HKUST-1 and MIL-101, Effect of Textural Properties on the Adsorption and Desorption of Toluene on the Metal-Organic Frameworks HKUST-1 and MIL-101,” Adsorption Science & Technology, vol. 31, no. 4, pp. 325–339, Apr. 2013.

[33] D. Peralta et al., “Adsorption and Separation of Xylene Isomers: CPO-27-Ni vs HKUST-1 vs NaY,” The Journal of Physical Chemistry C, vol. 116, no. 41, pp. 21844–21855, Oct. 2012.

[34] Y. Li et al., “Mechanochemical synthesis of Cu-BTC@GO with enhanced water stability and toluene adsorption capacity,” Chemical Engineering Journal, vol. 298, pp. 191–197, Aug. 2016.

[35] Z. Zhao, S. Wang, Y. Yang, X. Li, J. Li, and Z. Li, “Competitive adsorption and selectivity of benzene and water vapor on the microporous metal organic frameworks (HKUST-1),” Chemical Engineering Journal, vol. 259, pp. 79–89, Jan. 2015.

[36] D. A. Sarigiannis, S. P. Karakitsios, A. Gotti, I. L. Liakos, and A. Katsoyiannis, “Exposure to major volatile organic compounds and carbonyls in European indoor environments and associated health risk,” Environment International, vol. 37, no. 4, pp. 743–765, May 2011.

[37] K. Vellingiri et al., “Metal organic frameworks as sorption media for volatile and semi-volatile organic compounds at ambient conditions,” Sci Rep, vol. 6, p. 27813, 21 2016.

[38] K.-H. Kim, M.-H. Lee, and J. E. Szulejko, “Simulation of the breakthrough behavior of volatile organic compounds against sorbent tube sampler as a function of concentration level and sampling volume,” Analytica Chimica Acta, vol. 835, pp. 46–55, Jul. 2014.

[39] B. Tolnai, G. Barkó, J. Hlavay, and A. Gelencsér, “Evaluation of Carbopack B adsorbent for the tube-type diffusive sampling of volatile organic compounds at ambient concentration,” Analyst, vol. 124, no. 12, pp. 1859–1863, 1999.

[40] P. Ciccioli, E. Brancaleoni, A. Cecinato, C. di Palo, A. Brachetti, and A. Liberti, “Gas chromatographic evaluation of the organic components present in the atmosphere at trace levels with the aid of carbopack b for pre-concentration of the sample,” Journal of Chromatography A, vol. 351, pp. 433–449, Jan. 1986.

[41] I. Voiculescu, M. Zaghloul, and N. Narasimhan, “Microfabricated chemical preconcentrators for gas-phase microanalytical detection systems,” TrAC Trends in Analytical Chemistry, vol. 27, no. 4, pp. 327–343, Apr. 2008.

[42] J. Wang et al., “Belt-Mounted Micro-Gas-Chromatograph Prototype for Determining Personal Exposures to Volatile-Organic-Compound Mixture Components,” Anal. Chem., vol. 91, no. 7, pp. 4747–4754, Apr. 2019.

[43] Z. Cao et al., “Synthesis of mesoporous materials SBA-16 with different morphologies and their application in dibenzothiophene hydrodesulfurization,” Chemical Engineering Science, vol. 155, pp. 141–152, Nov. 2016.

[44] M. Jourshabani, A. Badiei, Z. Shariatinia, N. Lashgari, and G. Mohammadi Ziarani, “Fe-Supported SBA-16 Type Cagelike Mesoporous Silica with Enhanced Catalytic Activity for Direct Hydroxylation of Benzene to Phenol,” Ind. Eng. Chem. Res., vol. 55, no. 14, pp. 3900–3908, Apr. 2016.

[45] L. Kong et al., “Oxidative dehydrogenation of ethane to ethylene over Mo-incorporated mesoporous SBA-16 catalysts: The effect of MoOx dispersion,” Applied Catalysis A: General, vol. 510, pp. 84–97, Jan. 2016.

[46] K. Hamdi, M. Hébrant, P. Martin, B. Galland, and M. Etienne, “Mesoporous silica nanoparticle film as sorbent for in situ and real-time monitoring of volatile BTX (benzene, toluene and xylenes),” Sensors and Actuators B: Chemical, vol. 223, pp. 904–913, Feb. 2016.

[47] Y. Ueno, A. Tate, O. Niwa, H.-S. Zhou, T. Yamada, and I. Honma, “High benzene selectivity of mesoporous silicate for BTX gas sensing microfluidic devices,” Anal Bioanal Chem, vol. 382, no. 3, pp. 804–809, Jun. 2005.

[48] F. Luo et al., “Improved separation of micro gas chromatographic column using mesoporous silica as a stationary phase support,” Talanta, vol. 188, pp. 546–551, Oct. 2018.

[49] T. Granato, F. Testa, and R. Olivo, “Catalytic activity of HKUST-1 coated on ceramic foam,” Microporous and Mesoporous Materials, vol. 153, pp. 236–246, May 2012.

[50] J. Lee, O. K. Farha, J. Roberts, K. A. Scheidt, S. T. Nguyen, and J. T. Hupp, “Metal–organic framework materials as catalysts,” Chem. Soc. Rev., vol. 38, no. 5, pp. 1450–1459, Apr. 2009.

[51] I. Lara-Ibeas et al., “Sub-ppb Level Detection of BTEX Gaseous Mixtures with a Compact Prototype GC Equipped with a Preconcentration Unit,” Micromachines, vol. 10, no. 3, p. 187, Mar. 2019.

[52] J. Moellmer, A. Moeller, F. Dreisbach, R. Glaeser, and R. Staudt, “High pressure adsorption of hydrogen, nitrogen, carbon dioxide and methane on the metal–organic framework HKUST-1,” Microporous and Mesoporous Materials, vol. 138, no. 1–3, pp. 140–148, Feb. 2011.

[53] F. Raganati, V. Gargiulo, P. Ammendola, M. Alfe, and R. Chirone, “CO2 capture performance of HKUST-1 in a sound assisted fluidized bed,” Chemical Engineering Journal, vol. 239, pp. 75–86, Mar. 2014.

[54] A. Saito and H. C. Foley, “Argon porosimetry of selected molecular sieves: experiments and examination of the adapted Horvath-Kawazoe model,” Microporous Materials, vol. 3, no. 4–5, pp. 531–542, Jan. 1995.

[55] N. Al-Janabi et al., “Mapping the Cu-BTC metal–organic framework (HKUST-1) stability envelope in the presence of water vapour for CO2 adsorption from flue gases,” Chemical Engineering Journal, vol. 281, pp. 669–677, Dec. 2015.

[56] K.-S. Lin, A. K. Adhikari, C.-N. Ku, C.-L. Chiang, and H. Kuo, “Synthesis and characterization of porous HKUST-1 metal organic frameworks for hydrogen storage,” International Journal of Hydrogen Energy, vol. 37, no. 18, pp. 13865–13871, Sep. 2012.

[57] N. Lamia, M. Jorge, M. A. Granato, F. A. Almeida Paz, H. Chevreau, and A. E. Rodrigues, “Adsorption of propane, propylene and isobutane on a metal–organic framework: Molecular simulation and experiment,” Chemical Engineering Science, vol. 64, no. 14, pp. 3246–3259, Jul. 2009.

[58] Y. Zhai, B. Tu, and D. Zhao, “Organosilane-assisted synthesis of ordered mesoporous poly(furfuryl alcohol) composites,” J. Mater. Chem., vol. 19, no. 1, pp. 131–140, Dec. 2008.

[59] G. Autie-Castro, M. A. Autie, E. Rodríguez-Castellón, C. Aguirre, and E. Reguera, “Cu-BTC and Fe-BTC metal-organic frameworks: Role of the materials structural features on their performance for volatile hydrocarbons separation,” Colloids and Surfaces A: Physicochemical and Engineering Aspects, vol. 481, pp. 351–357, Sep. 2015.

[60] P. Küsgens et al., “Characterization of metal-organic frameworks by water adsorption,” Microporous and Mesoporous Materials, vol. 120, no. 3, pp. 325–330, Apr. 2009.

[61] Y.-K. Seo, G. Hundal, I. T. Jang, Y. K. Hwang, C.-H. Jun, and J.-S. Chang, “Microwave synthesis of hybrid inorganic–organic materials including porous Cu3(BTC)2 from Cu(II)-trimesate mixture,” Microporous and Mesoporous Materials, vol. 119, no. 1, pp. 331–337, Mar. 2009.

[62] N. L. Nagda and M. Hodgson, “Low relative humidity and aircraft cabin air quality,” Indoor Air, vol. 11, no. 3, pp. 200–214, Sep. 2001.

[63] A. Banerjee, U. Singh, V. Aravindan, M. Srinivasan, and S. Ogale, “Synthesis of CuO nanostructures from Cu-based metal organic framework (MOF-199) for application as anode for Li-ion batteries,” Nano Energy, vol. 2, no. 6, pp. 1158–1163, Nov. 2013.

[64] D. Farrusseng et al., “Heats of Adsorption for Seven Gases in Three Metal−Organic Frameworks: Systematic Comparison of Experiment and Simulation,” Langmuir, vol. 25, no. 13, pp. 7383–7388, Jul. 2009.

[65] X. Zhang et al., “Adsorption/desorption kinetics and breakthrough of gaseous toluene for modified microporous-mesoporous UiO-66 metal organic framework,” Journal of Hazardous Materials, vol. 366, pp. 140–150, Mar. 2019.

[66] J. H. Lee, S. A. Batterman, C. Jia, and S. Chernyak, “Ozone Artifacts and Carbonyl Measurements Using Tenax GR, Tenax TA, Carbopack B, and Carbopack X Adsorbents,” Journal of the Air & Waste Management Association, vol. 56, no. 11, pp. 1503–1517, Nov. 2006.

[67] A. Khan et al., “A comparison of figure of merit (FOM) for various materials in adsorptive removal of benzene under ambient temperature and pressure,” Environmental Research, vol. 168, pp. 96–108, Jan. 2019.

[68] D. Peralta et al., “Comparison of the Behavior of Metal–Organic Frameworks and Zeolites for Hydrocarbon Separations,” J. Am. Chem. Soc., vol. 134, no. 19, pp. 8115–8126, May 2012.

[69] R. Serna-Guerrero and A. Sayari, “Applications of Pore-Expanded Mesoporous Silica. 7. Adsorption of Volatile Organic Compounds,” Environ. Sci. Technol., vol. 41, no. 13, pp. 4761–4766, Jul. 2007.

[70] X. S. Zhao, G. Q. Lu, and X. Hu, “Organophilicity of MCM-41 adsorbents studied by adsorption and temperature-programmed desorption,” Colloids and Surfaces A: Physicochemical and Engineering Aspects, vol. 179, no. 2–3, pp. 261–269, Jan. 2001.

[71] D. Peralta et al., “Comparison of the Behavior of Metal–Organic Frameworks and Zeolites for Hydrocarbon Separations,” Journal of the American Chemical Society, vol. 134, no. 19, pp. 8115–8126, May 2012.

[72] D. Holmes Parker, M. E. Jones, and B. E. Koel, “Determination of the reaction order and activation energy for desorption kinetics using TPD spectra: Application to D2 desorption from Ag(111),” Surface Science, vol. 233, no. 1, pp. 65–73, Jul. 1990.

[73] Z. Zhang, S. Xian, H. Xi, H. Wang, and Z. Li, “Improvement of CO2 adsorption on ZIF-8 crystals modified by enhancing basicity of surface,” Chemical Engineering Science, vol. 66, no. 20, pp. 4878–4888, Oct. 2011.

[74] P. A. Redhead, “Thermal desorption of gases,” Vacuum, vol. 12, no. 4, pp. 203–211, Jul. 1962.

[75] F. Xu, S. Xian, Q. Xia, Y. Li, and Z. Li, “Effect of Textural Properties on the Adsorption and Desorption of Toluene on the Metal-Organic Frameworks HKUST-1 and MIL-101, Effect of Textural Properties on the Adsorption and Desorption of Toluene on the Metal-Organic Frameworks HKUST-1 and MIL-101,” Adsorption Science & Technology, vol. 31, no. 4, pp. 325–339, Apr. 2013.

[76] H. Pan, M. Xu, Z. Li, S. Huang, and C. He, “Catalytic combustion of styrene over copper-based catalyst: Inhibitory effect of water vapor,” Chemosphere, vol. 76, no. 5, pp. 721–726, Jul. 2009.